International Journal of Chemical, Materials and Biomolecular Sciences
ISSN: 2415-6620
Vol:6, No:11, 2012

Modeling of Fluid Flow in 2D Triangular, Sinusoidal, and Square Corrugated Channels

Abdulbasit G. A. Abdulsayid

***Abstract*—**The main focus of the work was concerned with hydrodynamic and thermal analysis of the plate heat exchanger channel with corrugation patterns suggested to be triangular, sinusoidal, and square corrugation. This study was to numerically model and validate the triangular corrugated channel with dimensions/parameters taken from open literature, and then model/analyze both sinusoidal, and square corrugated channel referred to the triangular model. Initially, 2D modeling with local extensive analysis for triangular corrugated channel was carried out. By that, all local pressure drop, wall shear stress, friction factor, static temperature, heat flux, Nusselt number, and surface heat coefficient, were analyzed to interpret the hydrodynamic and thermal phenomena occurred in the flow. Furthermore, in order to facilitate confidence in this model, a comparison between the values predicted, and experimental results taken from literature for almost the same case, was done. Moreover, a holistic numerical study for sinusoidal and square channels together with global comparisons with triangular corrugation under the same condition, were handled. Later, a comparison between electric, and fluid cooling through varying the boundary condition was achieved. The constant wall temperature and constant wall heat flux boundary conditions were employed, and the different resulted Nusselt numbers as a consequence were justified. The results obtained can be used to come up with an optimal design, a 'compromise' between heat transfer and pressure drop.

***Keywords*—**Corrugated Channel – CFD - Heat Exchanger – Heat Enhancement.

I. Introduction

THE need for designing process equipment that complies with the principles of economic and achieving high efficiency acted as a driving force towards the evolution in the design of plate heat exchangers. The high heat transfer rates, and lower pressure drop, become pivotal functional requirements for an efficient design, which are greatly influenced by the pattern of plate. Reference [1] stipulated that generally there are two mechanisms for the augmentation of heat transfer. Those mechanisms are associated with friction expenditure which increases the pressure loss, flow separation, and reattachment processes. As the channel with complicated passage is formed as a result of the arrangement of the two plates, the breakup and reattachment of boundary layers together with vortices flows occurring in the passage, are the most affective contributes to the high heat transfer efficiency.

Abdulbasit Abdulsayid is with Sirte Oil Company, Benghazi, Libya (phone: 00218-91-7399392; fax: 00218-21-3605118; e-mail: mansorey@ yahoo.com).

However, due to substantial increase in pressure drop accompanied with heat transfer augmentation in corrugated walls channels, [2] insisted that an optimum design balancing between friction losses and heat transfer rates, had to be considered, while [3] recommended that the Reynolds numbers used in plate heat exchanger is required to be lower than those for shell and tube heat exchangers for the same flow rates, so that the acceptable pressure drops could be achieved. Hence, as the plate configuration has a massive influence upon the hydraulic and thermal performance of the heat exchanger, the final design is robustly relevant to the initial choice of the plate configuration. Recently, a great amount of research on heat exchangers has focused on generating different correlations between the Nusselt number and the friction factor, since these measures, as [4] mentioned, can be determined experimentally over the whole heat exchanger. Reference [5] investigated numerically the optimum geometrical and flow parameters for turbulent heat transfer in a two-dimensional serpentine channel with a series of right-angle turns for a fluid with Prandtl number varying from 7 – 0.7, and Reynolds number varying from 15000 – 60.000, where the findings were a significant heat transfer enhancement obtained by varying both Reynolds number and geometry parameters. Also, [6] numerically studied a channel, but this time with sinusoidal corrugation and at lower Reynolds number. The study focus was upon the steady and transitional-flow regime, in which, it was observed that the enhancement of heat transfer for the wavy channel was about 2.5 times and the friction factor was about twice for the parallel-plate channel imposed under the same conditions. Reference [7] studied numerically and experimentally the effect of three dimensional hydrodynamics on the enhancement of heat transfer in the corrugated channels. End result was that the breaking and destabilizing in the thermal boundary layer which was promoted as fluid flowing through the corrugated surface, affected positively the heat transfer rate. Reference [8] studied on the simulation and flow visualization on the dynamical behavior of vortices generated in channels where it was discovered that the channel geometries had an important effect of the flow characteristics. Reference [9] handled the corrugation channel with another application. The numerical study was conducted to examine the convection heat transfer inside the channel between the flat plated covered with sine wave absorber in a cross corrugated solar air heater. The results found that characteristic ratio of the channel height to the amplitude height of the sine wave absorber, the ratio of one-fourth of the wavelength to the amplitude height of the absorber, and the angle of inclination

of the heater, were the only variable parameters which control the heat transportation. Reference [10] studied effect of corrugation angle on the performance of the flowing between two identical APV SR3 plates. In this paper, the CFD calculations showed that the inclination angle between the plate corrugations and the overall flow direction was a major parameter in the thermohydraulic performance of plate heat exchangers. Reference [11] numerically investigated the two-dimensional time dependent fluid flow and heat transfer in two geometrical configurations for the unsteady regime with Reynolds number (175 to 200) for sinusoidal channel, and Reynolds number varying from 60 to 80 for the arc-shape channel. The results showed that as long as the heat transfer enhancement was high, the pressure loss was high too. Reference [12] studied effects of the inclination angle, the wavelength, the amplitude, and the shape of the corrugation on the heat and mass transfer of the heat exchanger. Reference [13] studied numerically on the fully unsteady fluid flow and heat transfer in sine shaped wavy channels. Reference [14] considered the influence of the sinusoidal wavy-surface plate-fin geometry on hydrodynamic and thermal behaviors of laminar air flow under a constant wall temperature and through the range of Reynolds number from 10 to 1000. The predicted results were identical to the results of the above mentioned researches. The vortices which were responsible for enhancing of heat transfer increased as the Reynolds number increased and with sharp and sudden sinusoidal corrugation. These results were approved under the same conditions by [15], but with viscous liquids (Pr 5, 35, and 150). Similarly to [14], [16] investigated the same model but changing flow type to force flow, and using both the constant wall temperature and constant wall heat flux as boundary conditions. However, the predicted flow phenomena were comparable, but the thermal performance with the constant heat flux was higher than that with constant temperature boundary condition. Under the same condition as above i.e. constant wall temperature and constant wall heat flux, [17] undertook a fully developed laminar water flow for sinusoidal channels of circular and semi-circular cross-section, and investigated the influence of Reynolds number *(*5<Re<200*)* and amplitude to half wavelength ratio *(*0.222<*A/L*<0.667*)* on heat transfer enhancement and pressure drop. With varying the Reynolds number and amplitude to half wavelength ratio, the enhancement efficiency obtained with as large as 1.8, and 1.5 for the circular and semi-circular section respectively. Reference [18] studied the effect of both Reynolds number and geometry parameters on flow and thermal characteristic for wavy fin-and-tube heat exchanger from the view point of field synergy principle. The author found that the numerical results obtained show that the heat transfer performance can suitably be described by the field synergy principle. The investigation of developing laminar forced convection and entropy generation in both double- and half-sine ducts subject to the variation of Reynolds number (86 to 2000) was numerically carried out by [19]. The findings were that the Nusselt number in double-sine ducts was higher than that in half-sine, whereas the entropy generation in half-sine duct was much higher in double-sine ducts. Reference [20] used the Large-eddy simulation together with dynamic modeling to examine 3D turbulent flow in wavy channels exposed to the variation of Reynolds number (750 to 4500), spacing ratio, and waviness aspect ratio. It was found that the spacing ratio played a key role to produce vortices, control turbulent kinetic energy. And also, the friction factor was highly sensitive to the variation of spacing ratio. Reference [21] studied the design data and flow patterns for three types of offset fins and sixteen types of wavy fins for a compact plate heat exchanger. This study addressed the quantification of geometry generating maldistribution. The type of flow inside the corrugated channel in the compact heat exchanger as function of Reynolds number is a significant issue. Reference [22] mentioned again that the pertinent range of Reynolds number for the compact heat exchanger was between 500 and 15,000. Reference [23] who utilized the electrochemical mass transfer technique to calculate values of the local transfer coefficient for a corrugated plate heat exchanger channel, confirmed that the pure laminar flow did not exist for the tested Reynolds number range from 150 to 11,500. Also, it worth noting that when the compact heat exchangers were used as reflux condenser, [24] suggested that the limit imposed by the onset of flooding, reduces the Reynolds number for less than 2000. Reference [25], who experimentally tested a plate heat exchanger under two-phase flow conditions and visualized the flow regime, validated that the flow was turbulent for Re 650. Furthermore, [26], who studied experimentally the flow in narrow passages during counter-current gas–liquid flow, recommended that for gas Reynolds numbers in the range of 500–1300, the flow exhibited the basic features of turbulent flow.

In spite the fact that there have been numerous numerical studies concerning the heat transfer and pressure drop in the corrugated surface as a function of parametric variation for individual surface pattern. However, very rare works reported on heat transfer characteristics and pressure drop through corrugated channels with different surface patterns. Hence, the objective of this work is to provide a comparison study with different surface patterns so the researcher(s) develop an optimization method to select the efficient solution.

II. Numerical Method and Model Description

A Governing Equations

A Standard Computational Fluid Dynamic approach has been considered for this study. The method involves solution of the governing differential equations which were fully described by [27]. For our case, the main governing equations are stipulated as of [28], but as the k-ε Realizable model, is being used; the modeled transport equation for ε is modified based on [29]. Then, the main governing equations can be written in the following form:

Continuity Equation:

$$\frac{\partial \rho}{dt} + div(\rho U) = 0 \quad (1)$$

Momentum Equation:

x – Momentum: $\rho\frac{Du}{Dt} = -\frac{\partial p}{\partial x} + div(\mu\ grad\ u) + SMx$ (2)

y – Momentum: $\rho\frac{Dv}{Dt} = -\frac{\partial p}{\partial y} + div(\mu\ grad\ v) + SMy$ (3)

Energy Equation:

$\rho\frac{Di}{Dt} = -pdiv\ U + div(\Gamma\ grad\ T) + \phi + Si$ (4)

Turbulent Kinetic Energy (k)Equation:

$\frac{\partial(\rho K)}{\partial t} + div(\rho KU) = div\left[\left(\frac{\mu t}{\sigma K} grad\ K\right)\right] + 2\mu t Eij.Eij - \rho\varepsilon$ (5)

Turbulent Kinetic Energy Dissipation (ε)Equation:

$\frac{\partial(\rho\varepsilon)}{\partial t} + div(\rho\varepsilon U) = div\left[\left(\frac{\mu t}{\sigma\varepsilon} grad\ \varepsilon\right)\right] + C\ \rho\frac{\varepsilon^2}{K+\sqrt{v\varepsilon}}$ (6)

where

$\mu t = \rho C\mu K$

$C\mu$:A function of the mean strain and rotation rates, the angular velocity of the rotation system, and the turbulence fields.

c =1.9

$\sigma\varepsilon$ =1.2

σk =1

B. Methods of Calculation

In this study, the solution of the governing equations within the boundary conditions were presented in terms of pressure drop, wall shear stress, friction factor, turbulence intensity, heat flux, Nusselt number, and thickness of thermal boundary layer. The methods of calculations for the mentioned terms, as [30]–[31] defined and derived, are locally presented hereinafter, but together with our assumptions and simplifications:

Fluid Flow:

Reynolds Number:

Reynolds number is the ratio of inertial forces to viscous forces for the fluid flow. It can be expressed ad follow:

$$R_e = \frac{\rho u_{m D_h}}{\mu}$$

where,

D_h: Hydraulic diameter, which equals to $2h$ as [3] suggested.

h: Height of channel

Pressure Drop:

As the pressure drop results from both the wall shear and change in momentum flow rate cross the channel, so the pressure drop can be expressed as follow:

$$\Delta p = \left(\frac{\rho {u_m}^2}{2}\right) f\frac{L}{r_h}$$

where,

ρ: Fluid density

u_m: Average velocity

f: Friction factor

L: Length of channel

r_h: Half of channel height

Wall Shear Stress:

The shear stress results in the viscous forces created between the fluid layers in normal direction.

$$\tau = \mu\frac{du}{dy}$$

where,

μ: Dynamic viscosity

$\frac{du}{dy}$: Normal velocity gradient.

Friction Factor:

The friction factor is the ratio of wall shear stress to the kinetic energy per unit volume. It can be expressed as follow:

$$f = \frac{\tau}{\frac{\rho {u_m}^2}{2}}$$

where,

τ: Shear stress

Turbulence Intensity:

Turbulence intensity is the ratio of the root mean square of the turbulence velocity fluctuation at particular location to the average of the velocity at the same location. It can be expressed as follow:

$$T.I = \frac{u'}{u_m}$$

where,

u': The turbulence velocity

Heat Transfer:

Heat Flux:

For simplification, the heat flux is assumed to be related to the inlet temperature and wall temperature instead to be related to bulk temperature. Then, it can be expressed as follow:

$$q = h_l(T_{inlet} - T_w)$$

where,

h_l: Surface coefficient factor

T_{inlet}: Inlet temperature

T_w: Wall temperature

Nusselt Number:

Nusselt number is the ratio of convective to conductive heat transfer cross the boundary layer. It can be expressed as follow:

$$Nu = \frac{q\ h}{(T_{inlet} - T_w)K}$$

where,

h: Height of channel
K: Thermal conductivity of the fluid

Thickness of Thermal Boundary Layer:

The thickness of thermal boundary layer can be obtained from the following empirical equation:

$$\delta = \left(\frac{5x}{R_e^{0.5}}\right)\left(\frac{1}{1.026}P_r^{\frac{-1}{3}}\right)$$

where,

x: Local channel length
P_r: Prandtl number

C Numerical Analysis

Statement of Problem:

The geometries studied in these simulations are as follow:

-An existing compact heat exchanger handled numerically by [2], and experimentally by [25], with some modifications stated hereinafter. The geometry, which creates a triangular vertical channel of a corrugated plate heat exchanger, is formed by two plates, 70 cm high and 15 cm wide. On each plate, the inclination angles are suggested to be a 45°. The two plates are superposed in the way that the opposite corrugations formed a cross-type pattern where the peaks and valleys in the top and bottom-plates lie on the same longitudinal plane. The geometry is consisted of fourteen equal sized and uniformly spaced corrugations and two side-channels as illustrated and detailed in Fig. 1, and Table I. However, this study is carried out for a single phase flow of water.

-A Sinusoidal vertical channel of a corrugated plate heat exchanger. The geometry specification is similar to the above mentioned case, but the configuration of the valleys and peaks are sinusoidal as shown in Fig.2.

-Square vertical channel of a corrugated plate heat exchanger. The geometry specification is similar to the above mentioned cases, but the configuration of the valleys and peaks are squares as shown in Fig.3.

TABLE I
PLATE DIMENSIONS

Plate Parameter	Dimension
Plate length	0.200 m
Plate width	0.110 m
Maximum spacing between plates, d	0.010 m
Number of corrugations	14
Corrugation angle	45°
Corrugation pitch, h	0.005 m
Corrugation width, w	0.014 m
Plate length before and after corrugations	0.050 m

The simulations were performed for a Reynolds number of 400, 900, 1000, 1150, 1250, and 1400, corresponding to an inlet water velocity of 0.02008, 0.04518, 0.0502, 0.05773, 0.06275, and 0.07028 m/s, for the case of hot water (60°C) in contact with both a constant-temperature wall (20°C) and a constant heat flux wall of 13593.02 W/m² for the triangular corrugated channel, 13846.93 W/m² for the sinusoidal corrugated channel, and 43589.336 W/m² for the square corrugated channel. The reason of using those particular heat fluxes was to keep the heat transported corresponding to each constant wall temperature case unchanging. However, to facilitate the accuracy, those values were computed by Fluent instead of being calculated by Trapezoidal integration rule.

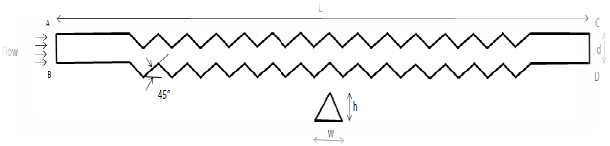

Fig. 1 Triangular corrugated channel

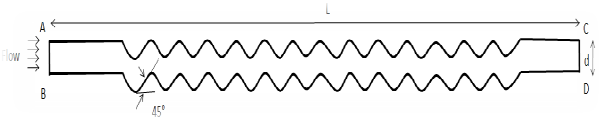

Fig. 2 Sinusoidal corrugated channel

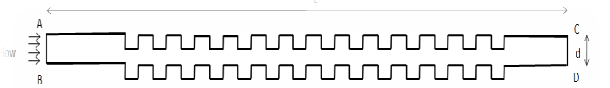

Fig. 3 Square corrugated channel

Boundary Condition

The boundary conditions applied to the 2D corrugated channels were divided to two cases:

-Constant temperature on the wall:

The mean velocity, and temperature of the uniform inflow of water were applied as boundary condition at the channel entrance. At the outflow boundary, the outlet pressure was set as an atmospheric. At upper and lower corrugated channel, no-slip conditions and constant wall temperature were specified.

With reference to Fig., 2, and 3, the detailed boundary conditions are shown as follow:

Inflow boundary, AB: $u = ui$
$T = Ti$
Outflow boundary, CD: $P = 0$
Wall boundary, AC, BD $u = v = 0$
$T = Tw$

-Constant heat flux on the wall:

As stated above, the mean velocity, and temperature of the uniform inflow of water were applied as boundary condition at the channel entrance. At the outflow boundary, the outlet pressure was set as an atmospheric. At upper and lower corrugated channel, no-slip conditions and constant wall heat flux were specified.

Similarly to constant wall temperature, the detailed boundary conditions for constant heat flux are shown as follow:

Inflow boundary, AB: $u = ui$
$T = Ti$
Outflow boundary, CD: $P = 0$
Wall boundary, AC, BD $u = v = 0$
$q = qw$

Computational Detail

In order to simulate and compute the detailed characteristics of the fluid flow corrugated channels problem, a commercial CFD codes, namely GAMBIT 2.0 (the pre-processor), and FLUENT 6.3 software package, were employed.

The geometry and grid generation was achieved by GAMBIT while the problems solutions were attained by FLUENT.

The fluid flow governing equations were solved by using the finite volume method.

The simulation was performed in 2D space, segregated solver, steady state flow, and absolute velocity formulation. With the interest of solving the temperature distribution, the energy equation was solved. The K-epsilon turbulence model was selected. With the purpose of producing more accurate results for boundary layers flow as confirmed by all of [32]- [33]- [34]- [35], the Realizable K-epsilon model was employed. And also, to facilitate a good handling of near wall features, the Enhanced Wall Treatment was chosen.

While, the convection scheme of density, momentum, turbulence kinetic energy, turbulence dissipation rate, and energy was taken as a first order upwind, pressure and pressure-velocity coupling were set to standard and simple methods respectively.

The residual under convergence criterion for continuity, x-velocity, y-velocity, energy, and epsilon were all set to 0.001.

The computation for triangular, sinusoidal, and square corrugated channels were performed with grid (56400 cells, 113800 faces, 57401, nodes, and 1 partition), (57900 cells, 116825 faces, 58926 nodes, and 1 partition), and (118400 cells, 239480 faces, 121081 nodes, and 1 partition) respectively. Owning to get more accurate results in the boundary layers, the grids were refined near the channel wall.

It is observed that the values of convergence criterion were dependent on the Reynolds number, and also, found that the solutions were converged for not less than 1 x 10 $^{-3}$. Fig.4 shows conversion chart for triangular corrugated channel at Re 400 for constant wall temperature. Finally, the number of iteration was found to be sensitive to the Reynolds number. As Reynolds number increased, the number of iteration decreased. Fig.5 demonstrates the correlation between the Reynolds number and the number of iteration for the triangular corrugated channel.

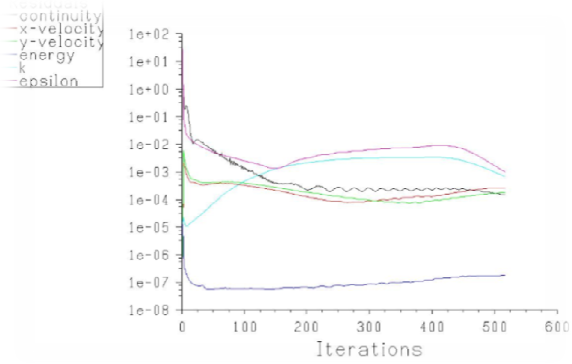

Fig. 4 Conversion chart

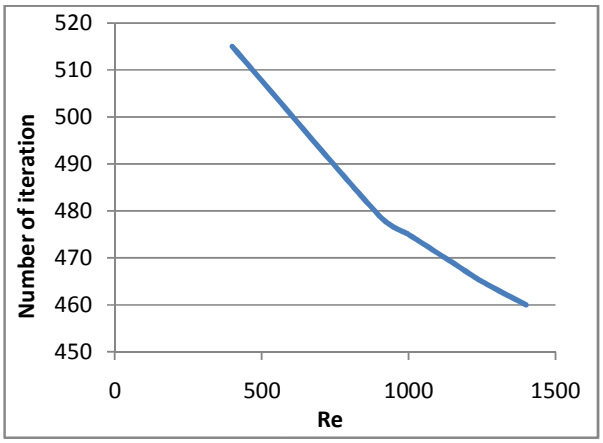

Fig. 5 Iteration Numbers vs Reynolds number

Grid Sensitivity

Altered grid arrangements were used for grid sensitivity test to simulate the triangular corrugated channel for Reynolds number of 400 in the case of constant wall temperature. The specification of the grids used are outlined in Table II, and depicted in Fig.6, 7, and 8.

TABLE II
GRIDS SPECIFICATION

Grid	Specification (Level x Cells x Faces x Nodes x Partition)	General Description
Coarse	39750 x 80345 x 40596 x 1	A hybrid grid is used in this problem, i.e. a structured quadratic (rectangular cells). For the case of boundary layer grid a successive ratio type is selected and set to 1.1. This treatment makes the cell size near the wall refined so that all the features in this region can be captured.
Fine regular	56400 x 113800 x 57401 x 1	
Fine boundary layer	56400 x 113800 x 57401 x 1	

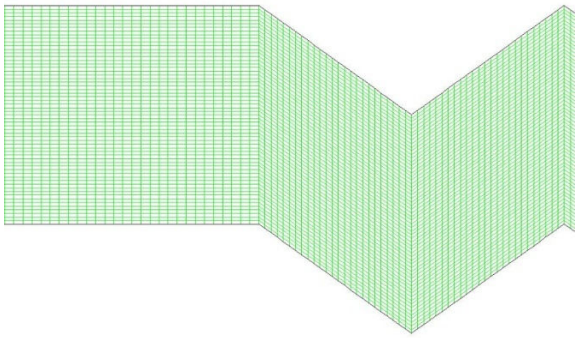

Fig. 6 Coarse grid

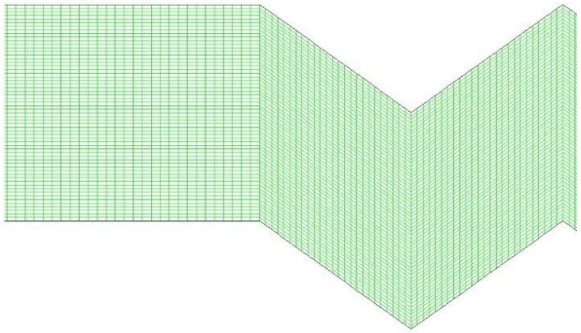

Fig. 7 Fine regular grid

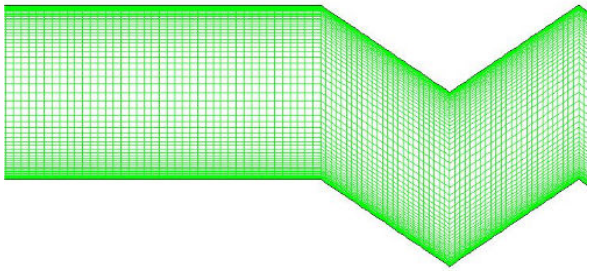

Fig. 8 Fine boundary layer grid

All the above grids were simulated. The maximum difference in the Nusselt number between the simulated grids and the results obtained by [2], is stated in the Table III.

From Table III, the fine boundary layer grid is chosen since it retains a high certain amount of accuracy. Thus, this meshing pattern is used to simulate both Triangular and Sinusoidal corrugated channels. For the Square corrugated channel, the strategy is to apply a mesh whose cells size is equal to the size of cells near the wall which is applied in the Triangular corrugated simulation. Fig. 9 and 10 show the configuration of mesh applied in sinusoidal, and square corrugated simulations.

TABLE III
GRIDS ACCURACY

Grid	Nusselt no.	Kanaris, Mouza, and Paras (Difference %)
Coarse	85	20.7 (310.5%)
Fine regular	54	20.7 (160%)
Fine boundary layer	22.25	20.7 (7.4%)

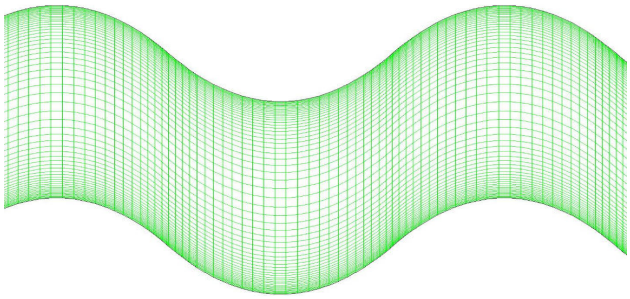

Fig. 9 Sinusoidal corrugated grid

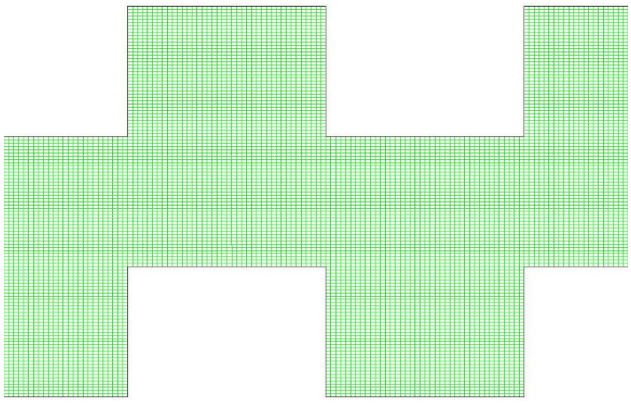

Fig. 10 Square corrugated grid

III. RESULTS AND DISCUSSION

Flow phenomena and heat transfer characteristics for constant wall temperature, were analyzed locally and globally with CFD code based modeling, giving important information about the effect of three geometries of corrugated channels on hydrodynamic and thermal behaviors of the flow crossing the channels.

Firstly, the velocity magnitude, static pressure, turbulence intensity, and temperature distribution within Reynolds number varying from 400 to 1400, were all presented and analyzed for the triangular corrugated channels. Moreover, gradient of pressure, shear stress, friction factor, total heat flux, Nusselt number, and the surface heat transfer coefficient for the lower plate of triangular corrugated channel were graphed and locally analyzed.

Then, in order to verify that the CFD code is an efficient and reliable tool for studying the effect of corrugation geometries upon the flow motion and heat transfer considerations, the code was validated by comparing the numerical results with experimental data on Nusselt number and friction factor acquired for corrugated plates imposed under almost the same conditions.

Afterwards, similarly to the triangular corrugated case, the velocity magnitude, static pressure, turbulence intensity, and total temperature distribution within the same variation of Reynolds number, were presented for both the sinusoidal, and square corrugated channels.

Later, global comparisons between the three corrugated channels in pressure drop, wall shear stress, friction factor, heat flux, Nusselt number, and surface heat transfer coefficient, for the lower plate for each channel, were presented.

Finally, the Nusselt numbers for both fluid cooling and electric cooling i.e. Constant wall temperature and constant wall heat flux respectively, were compared and analyzed.

A. Results Predicted for Triangular Corrugated Channel

Hydrodynamic Prediction

Fig.11 and 12 show the flow motion represented in velocity magnitude for both Reynolds numbers 400, and 1400.

It can be seen that the main flow deflects into the corrugated confined area where the vortices are created. The vortex grows larger and its centre moves to the downstream as Reynolds number increases, and occupies the confined area. The vortices in the confined corrugated area repeat the propagation that they travel to the downstream simultaneously in the lower and upper plates.

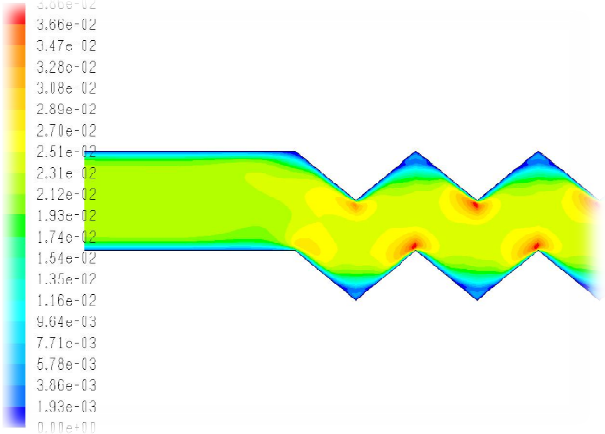

Fig. 11 Velocity magnitude at Re 400

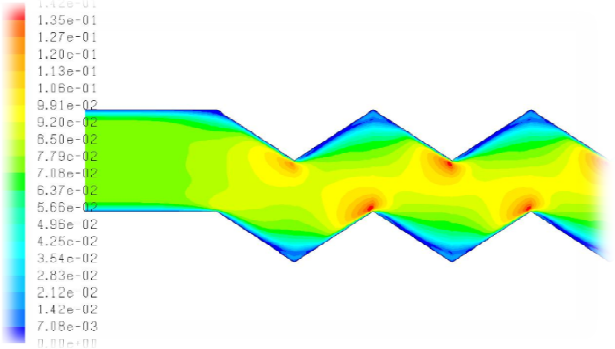

Fig. 12 Velocity magnitude at Re 1400

The phenomena of the creation of vortex in the channel can be qualitatively interpreted to the pressure gradients within the periodic corrugation. Fig. 13 represents the pressure gradients through two periodic corrugations where the first peak is located at 0.5 cm from the total length of the channel and second and third peaks are settled at 0.64, a0.78 cm respectively. Similarly, the relevant valleys are positioned at 0.57, and 0.71 cm. As the flow progress along the corrugation, the pressure decreases through the entrance flat channel, and then increases gradually when the flow passes from the peak to the valley. And, correspondingly, the pressure decreases again when the flow elapses from valley to peak. This behavior of pressure repeats itself for the second corrugation. This fluctuation of the pressure is a function of wall shear stress variation as it can be seen later and to the variation of cross sectional area. Seeing that the increase of pressure and reduction in velocity are related through the Bernoulli equation, the increasing of pressure causes a reduction in velocity, and when the momentum of the fluid layers near the surface is not sufficiently high to overcome the increase in pressure, the velocity gradient at the surface comes to zero where the boundary layer of the flow reaches the separation point. As the flow progresses beyond the separation point, clockwise rotated reverse flow occurs. This flow is characterized by turbulent and random motion. When the flow moves from valley to peak, the pressure is getting reduced as the velocity increases. As the velocity at the surface comes to zero again the reattachment of boundary layer occurs. All of these phenomena are depicted in Fig.14.

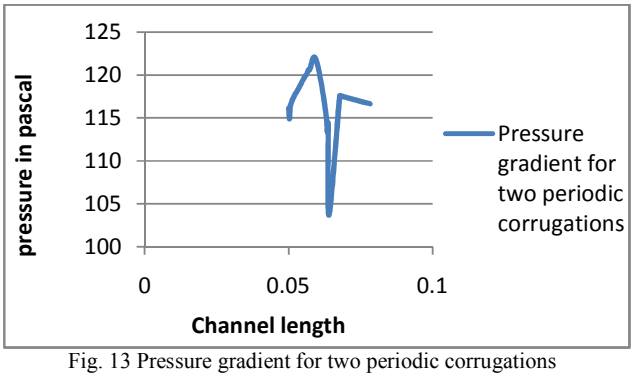

Fig. 13 Pressure gradient for two periodic corrugations

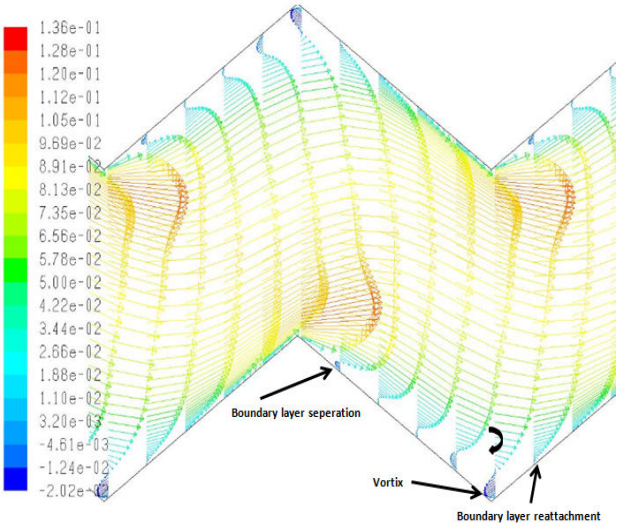

Fig. 14 Vector of velocity magnitude at Re 1400

Fig. 15 and 16 show the static pressure in Pascal for the triangular corrugation channel for both Reynolds numbers 400 and 1400. The figures show that the rate of the decrease of pressure is almost evenly either the Reynolds number low or high.

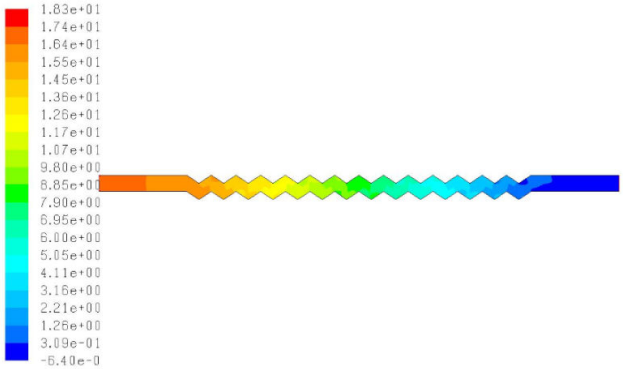

Fig. 15 Static pressure at Re 400

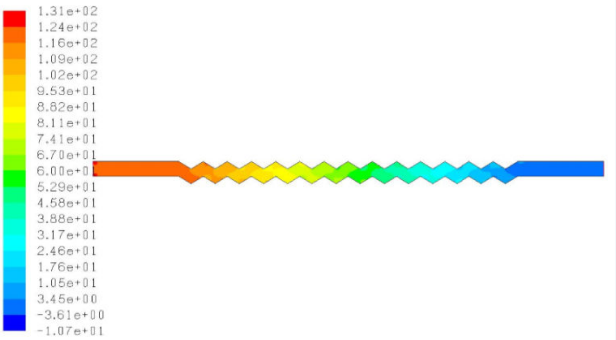

Fig. 16 Static pressure at Re 1400

Fig. 17 compares the local pressure gradients for the triangular corrugation channel for Reynolds numbers varying from 400 to 1400. It can be seen that as the Reynolds number increases the pressure drop increases.

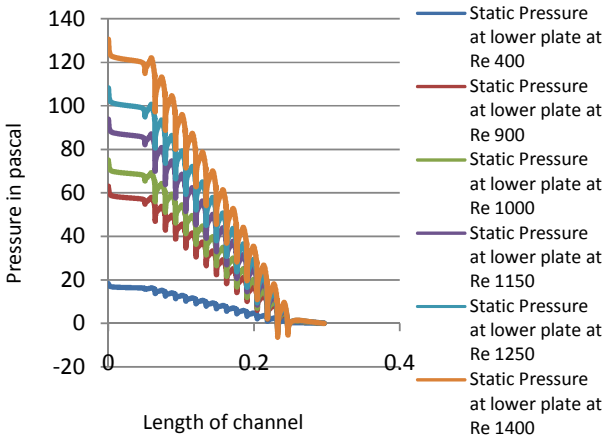

Fig. 17 Local pressure gradient for triangular corrugated channel

The most salient feature in the plot is that the series of periodic changes in flow direction induces a significant resistance to the flow and increases the pressure drop which in turn increases the friction losses. Moreover, the increase of pressure drop has a trade off with the increment of the flow velocity. As the inlet velocity increases 125% the pressure drop increases 233.3%. Fig.18 and 19 show the turbulence intensity in percentage for the triangular corrugation channel for both Reynolds numbers 400 and 1400.

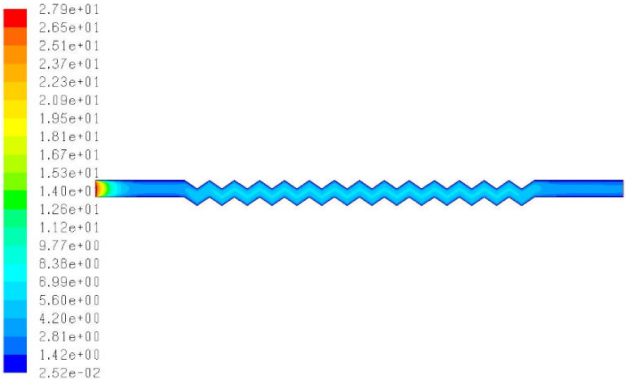

Fig.18 Turbulence intensity at Re 400

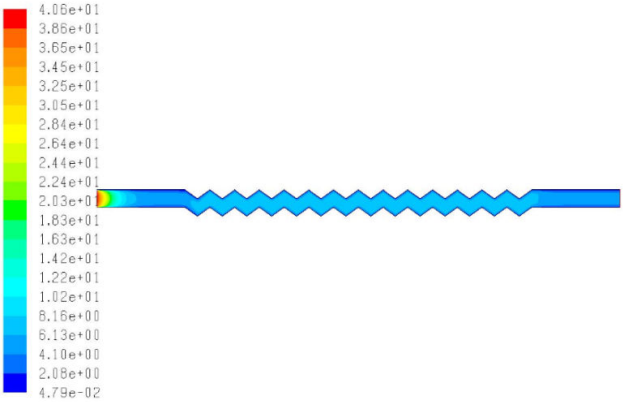

Fig. 19 Turbulence intensity at Re 1400

The most important feature in the figures is that the turbulence intensity abruptly increases at the entrance, and then decreases along the flat plate channels. Afterwards, the intensity increases and remains constant all along the corrugated plate channel before it decreases again at the flat plate at the outlet of the channel.

Furthermore, it is noticeable that the turbulence intensity is sensitive to the variation of Reynolds number. As Reynolds number increases the intensity increases as a consequence. At the same time as the velocity rises to 250% at the second valley of the channel, the turbulence intensity climbs from 8.3% to 16.3%.

Fig. 20 represents the local shear stress in Pascal for the lower plate of the triangular corrugated channel for the Reynolds number varying from 400 to 1400.

It is prudent that as Reynolds number increases the shear stress increases as well. Also, it can be seen that the areas in which the shear stress is high is the same area in which the pressure drop is high too. To be more accurate, the shear stress reaches the highest value at the peak of corrugation as shown in Fig.21.

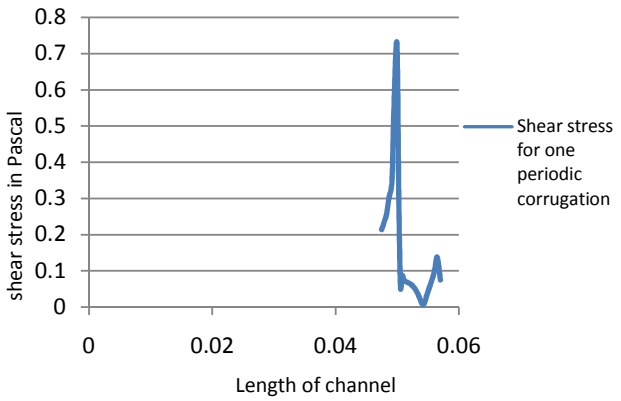

Fig. 20 Local shear stress for triangular corrugated channel

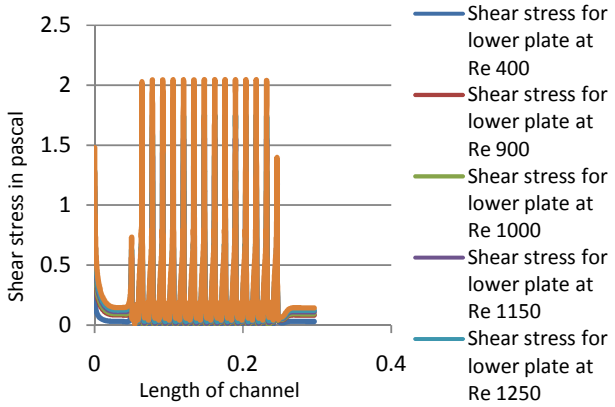

Fig. 21 Shear stress for one periodic corrugation

This can be justified that in this particular area the change in moment flow rate as velocity profile develops, reaches its maximum value at the corrugation peak before it starts decreasing again.

Fig. 22 denotes the local dimensionless friction factor for the lower plate of the triangular corrugated channel for the Reynolds number varying from 400 to 1400.

The important feature is that as the Reynolds number increases the friction factor decreases. This can be interpreted that as the friction factor is the ratio of wall shear stress to the flow kinetic energy per unit volume, and while the Reynolds number increases, both the wall shear stress, and the flow kinetic energy (function of velocity), increase, but the growth rate of the flow kinetic energy is bigger than of shear stress, so as a consequence, the friction factor decreases.

Another feature is that the highest value of friction factor occurs at the peak of corrugation as depicted in Fig. 23.

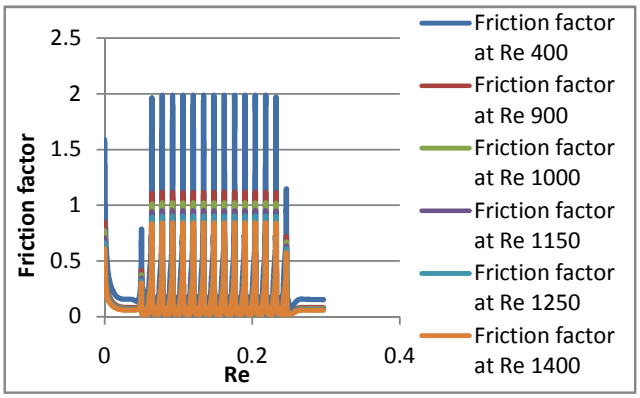

Fig. 22 Local friction factor for triangular corrugated channel

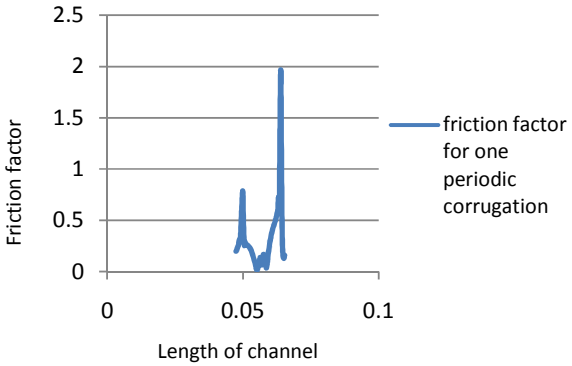

Fig. 23 Friction factor for one periodic corrugation

Thermal Prediction

Fig. 24 and 25 show the static temperature along the triangular corrugated channel for a constant wall temperature boundary condition at Reynolds numbers 400, and 1400.

The figures illustrate that the water cools gradually as it crosses the channel. Also, it is clear that the temperature difference is quite high in the corrugated area compared to the flat entrance and exit. This is displayed more obviously in the Fig. 26.

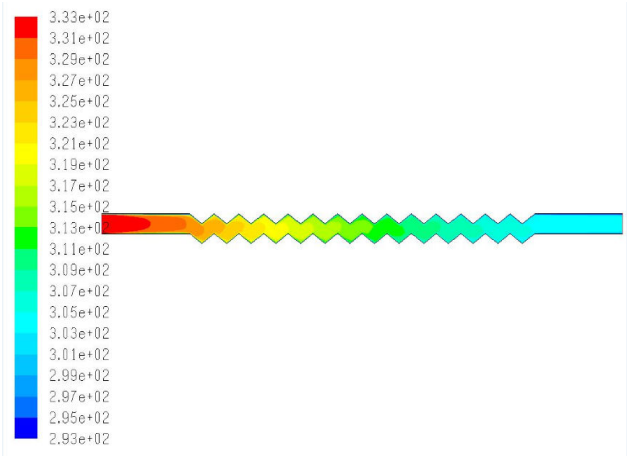

Fig. 24 Static temperature at Re 400

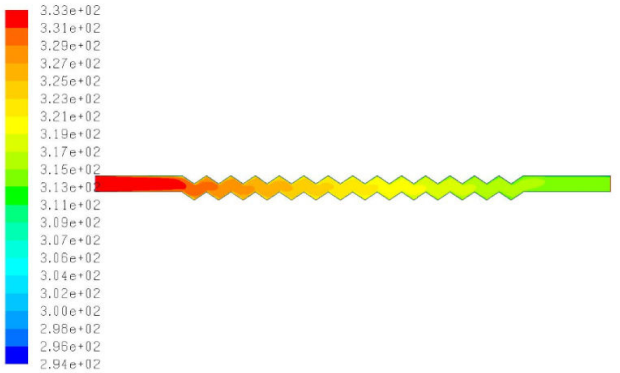

Fig. 25 Static temperature at Re 1400

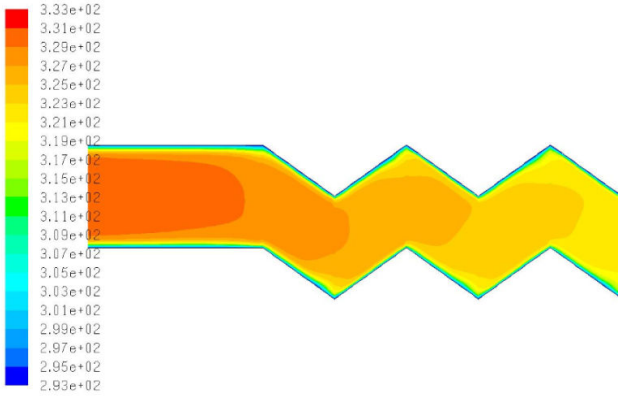

Fig. 26 Static temperature at the entrance part of the channel at Re 400

Fig. 27 exhibits the local heat flux in W/m2 for the triangular corrugated channel for the lower plate at Reynolds number changing from 400 t0 1400. The graph shows that with progression of Reynolds number, the rate of total heat flux increases.

The noticeable feature is that the heat flux slumps cross the flat plate before it fluctuates through the corrugated channel.

In addition, it is also obvious that the heat flux is quite high at the peak of corrugation. This is shown in Fig.28.

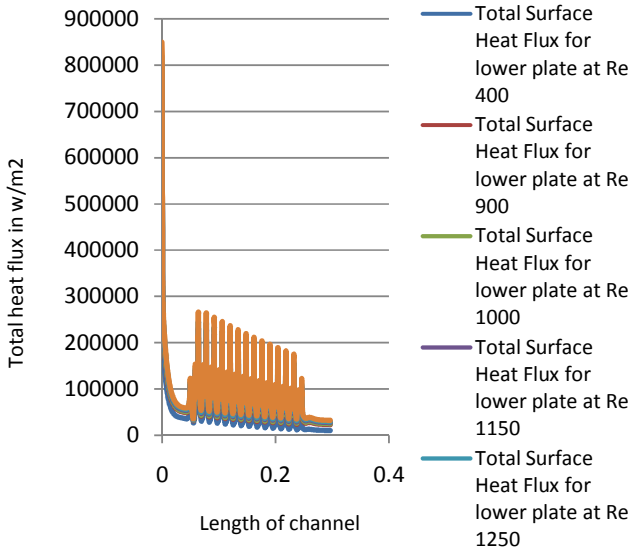

Fig. 27 Local total heat flux for triangular corrugated channel

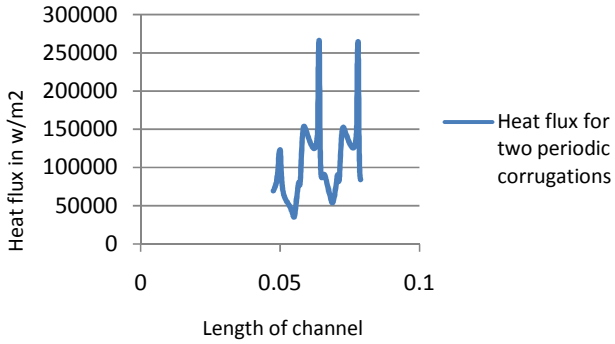

Fig. 28 Heat flux for two periodic corrugations

As the heat flux is related to both Nusselt number and heat coefficient, Fig. 29, and 30 show the identical behavior.

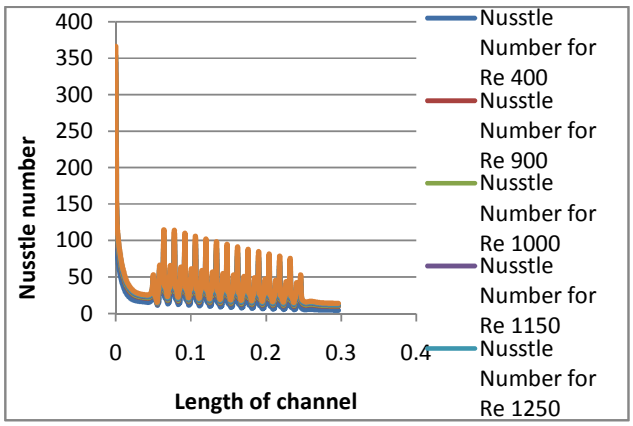

Fig. 29 Local Nusselt number for triangular corrugated channel

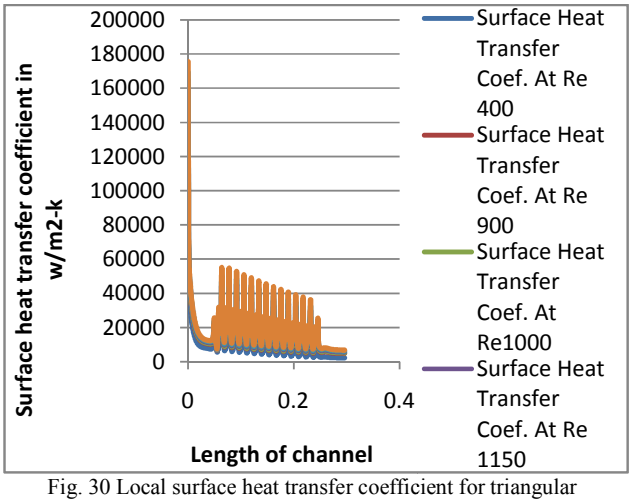

Fig. 30 Local surface heat transfer coefficient for triangular corrugated channel

The fluctuation of heat flux, and then the Nusselt number and surface heat coefficient can be elucidated and illustrated by Fig.31 and 32 hereinafter.

It can be seen that the main rationale for this phenomenon is the presence of vortices. As the vortex rotates clock wisely the water at the upstream of stagnation point is pushed away from the heated lower wall. On the other hand, the water near the downstream of stagnation point fluid is pushed toward the wall so that both temperature gradient and the velocity normal to the wall are significant. Thus, the heat flux along the lower wall near the upstream of stagnation point is lower than that of downstream. This explanation is presented by fluctuation of Nusselt number around the stagnation point.

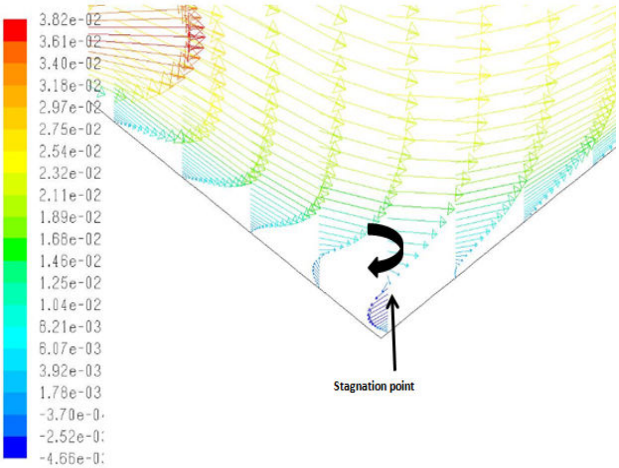

Fig. 31 Stagnation point

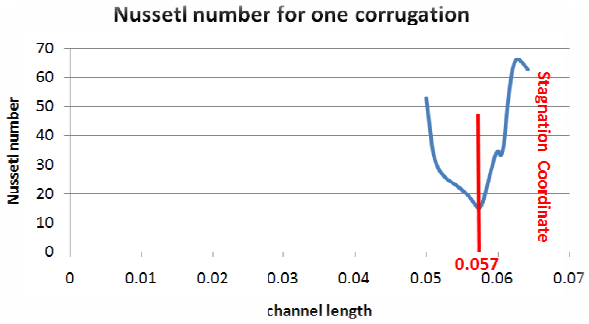

Fig. 32 Nusselt number around stagnation point

B. Validation of Triangular Corrugated Channel Model

Nusselt Number

The validity of the simulated Nusselt number is checked using experimental data achieved by [36]- [25]. It is also compared with the experimental values estimated by [3] . The simulated Nusselt number refers to a plate heat exchanger channel as the one used in the model setup by [2] with the difference that the channel used for [3] is formed by only one triangular corrugated plate, while the other plate is flat, and the plate used by [36] is a sinusoidal pattern.

From Fig. 33, it is found that there is an excellent agreement with the experimental data (±0.7% to ±4.9%).

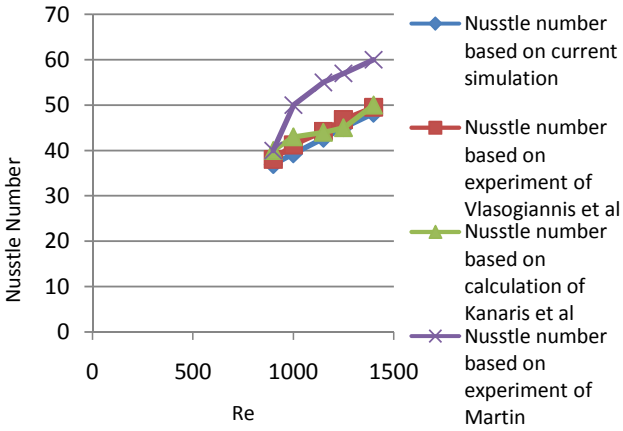

Fig. 33 Comparative plot between Nusselt number estimated by others and Nusselt number estimated by current estimation

Friction Factor

In a similar way, the validity of the simulated friction factor is checked using available experimental data attained by [2].

Fig. 34 shows that in spite of weakly agreement between the results, however, the results maintain almost the same slop.

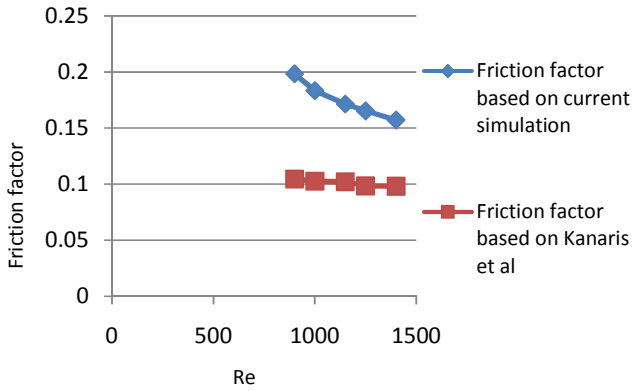

Fig. 34 Comparative plot between friction factor estimated by others and friction factor estimated by current estimation

C. Results Predicated for Sinusoidal Corrugated Channel

Fig. (36) and (37) show the flow motion represented in velocity magnitude for both Reynolds numbers 400, 1400.

Likewise to the triangular corrugated channel, the figures show that the vortices are created too, and the vortices grow larger and their centre move to the downstream as Reynolds number increases. But the vortices seem fractionally less than that created in triangular corrugated channel.

Fig. (38) and (39) show the static pressure in Pascal for the sinusoidal corrugation channel for both Reynolds numbers 400 and 1400. The figures illustrate that with the progression of Reynolds number, the pressure gradient goes up. Also, the pressure drop gradient in the sinusoidal corrugation is slightly less than the gradient in triangular corrugation.

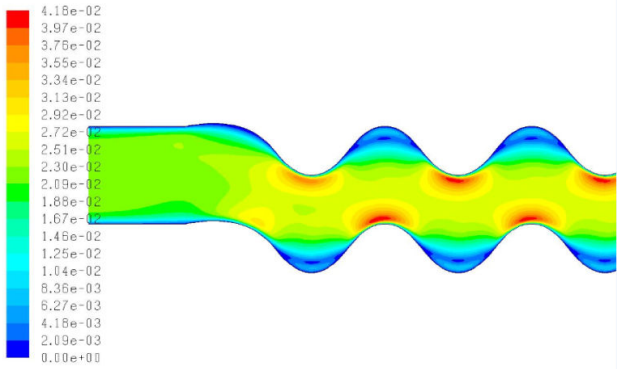

Fig. 35 Velocity magnitude at Re 400

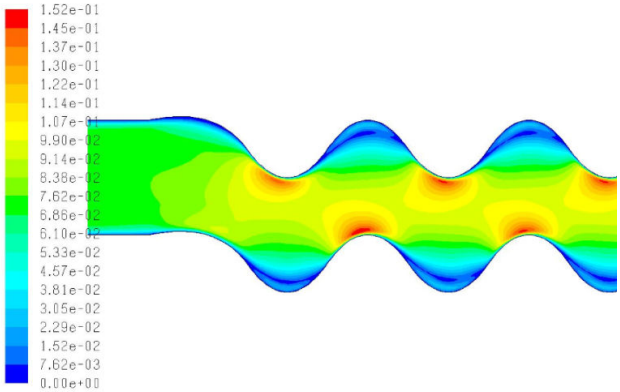

Fig. 36 Velocity magnitude at Re 1400

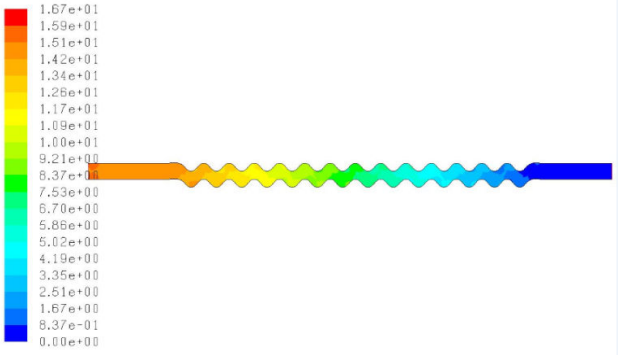

Fig. 37 Static pressure at Re 400

Fig. 39 and 40 show the turbulence intensity in percentage for the sinusoidal corrugation channel for both Reynolds numbers 400 and 1400. From the figures, it can be seen that there is an insignificant drop in turbulence intensity for the sinusoidal corrugation compared to triangular corrugation imposed under the same conditions.

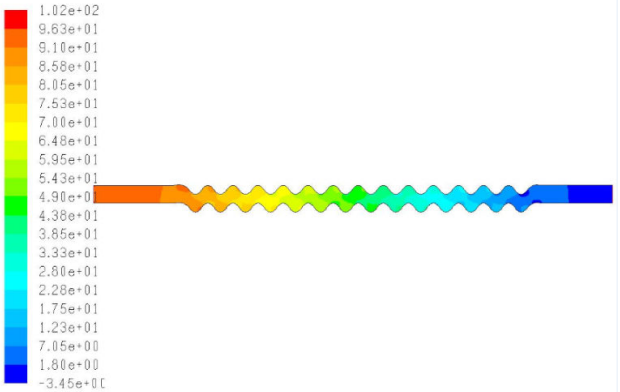

Fig. 38 Static pressure at Re 1400

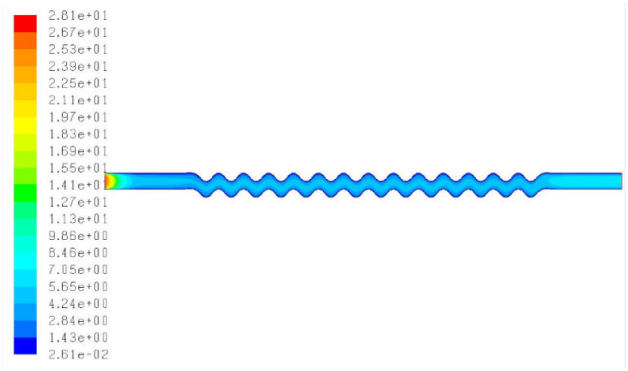

Fig. 39 Turbulence intensity at Re 400

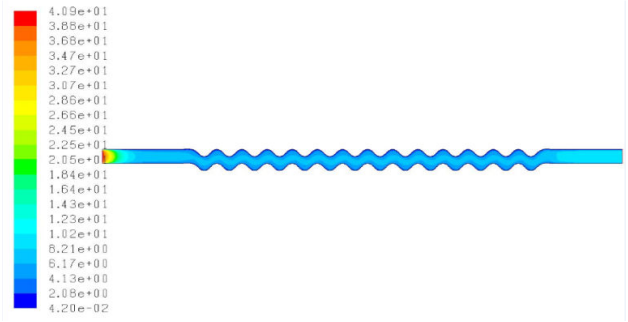

Fig. 40 Turbulence intensity at Re 1400

Fig. 41 and 42 show static temperature along the sinusoidal corrugated channel for a constant wall temperature boundary condition at Reynolds numbers 400, and 1400. The figures demonstrate that while the water passes through the channel, the changing in temperature becomes visible. Additionally, this change is significant in the confined areas as supplementary elucidated in Fig. 43.

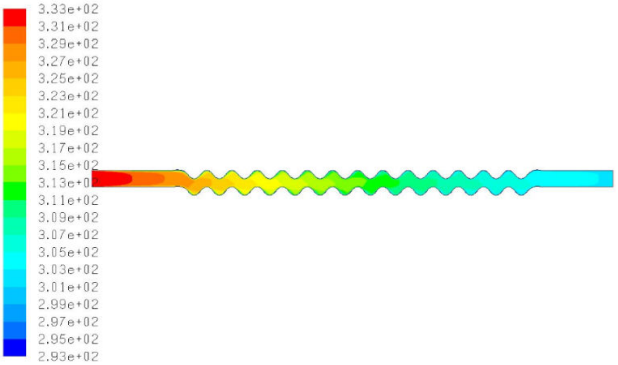

Fig. 41 Static temperature at Re 400

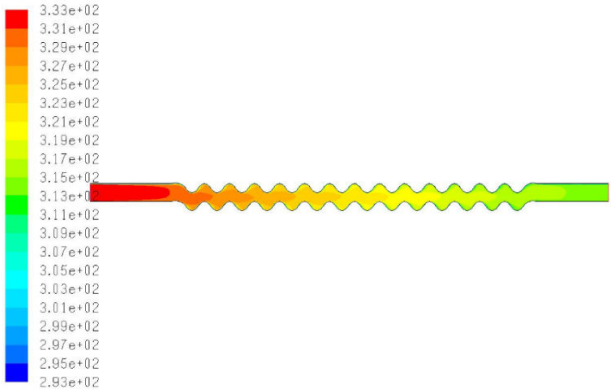

Fig. 42 Static temperature at Re 1400

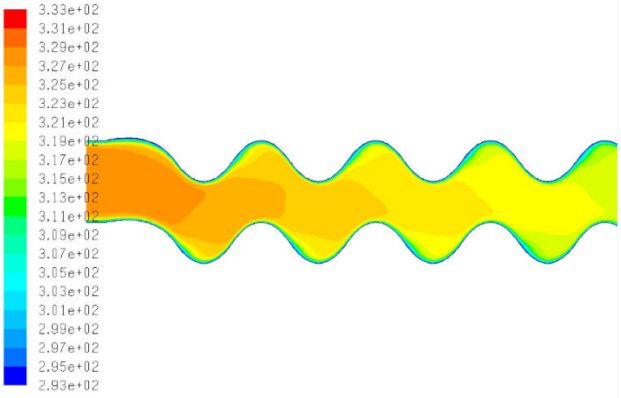

Fig. 43 Static temperature at the entrance part of the channel at Re 400

D.Results Predicated for Square Corrugated Channel

Fig. 44 and 45 show the velocity magnitude for both Reynolds numbers 400, 1400 for the square corrugated channel.

It is prudent that the vortices created in the confined areas are quite large compared to that created in either triangular or sinusoidal corrugation channel. This can be explained that the change in configuration of the square channel is more severe than of triangular and sinusoidal channels. As a consequence, the variation in both pressure and velocity gradient is substantial, thus, the reverse flow phenomena which create the vortices, occur exaggeratedly.

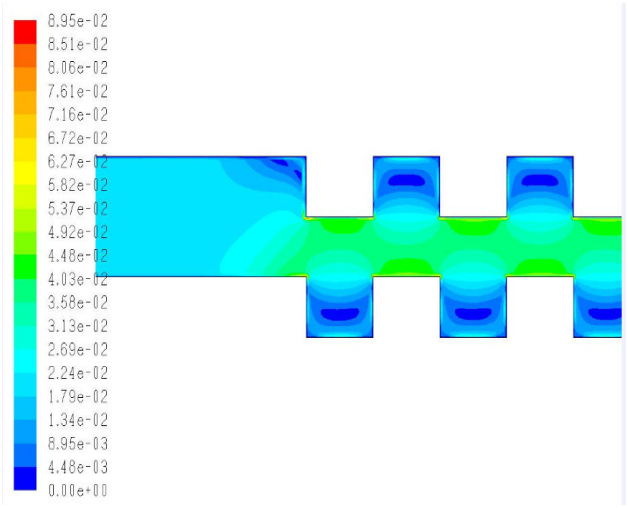

Fig. 44 Velocity magnitude at Re 400

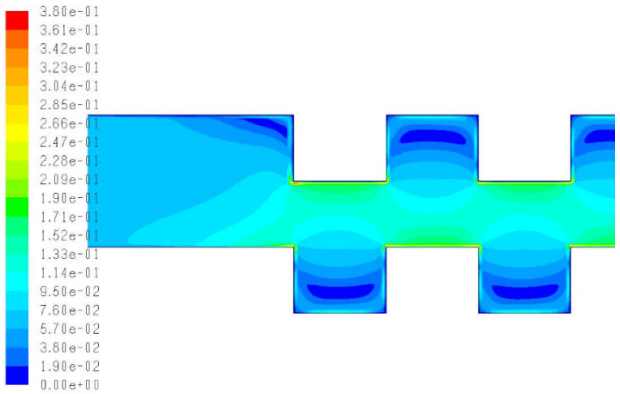

Fig. 45 Velocity magnitude at Re 1400

Fig. 46 and 47 show the static pressure in Pascal for the square corrugation channel for both Reynolds numbers 400 and 1400. As the sharpness of the corrugations for square channel is high, the rate pressure dropping as shown is considerably higher than the dropping in triangular and sinusoidal channels.

Fig. 48 and 49 show the static pressure in Pascal for the square corrugation channel for both Reynolds numbers 400 and 1400. As the sharpness of the corrugations for square channel is high, the rate pressure dropping as shown is considerably higher than the dropping in triangular and sinusoidal channels.

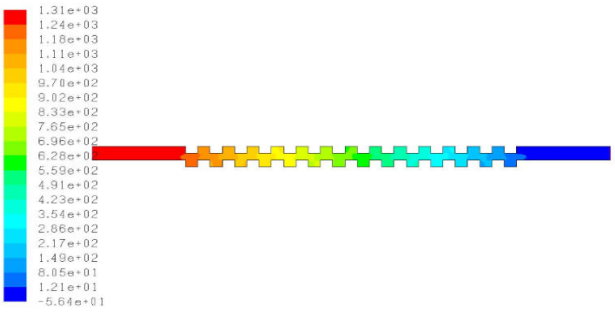

Fig. 46 Static pressure at Re 400

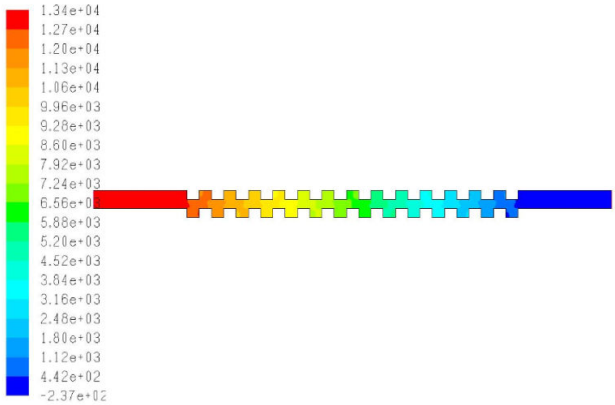

Fig. 47 Static pressure at Re 1400

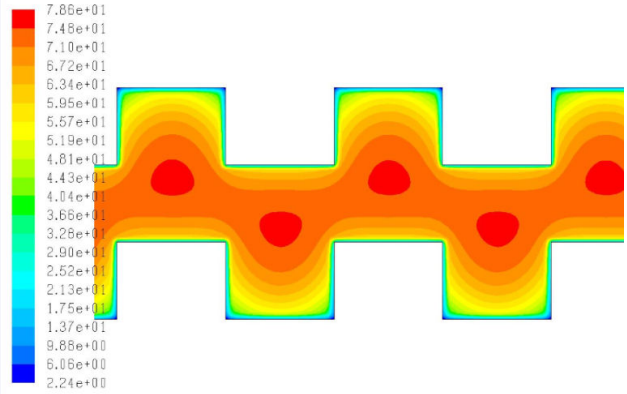

Fig. 48 Turbulence intensity at the middle of channel at Re 400

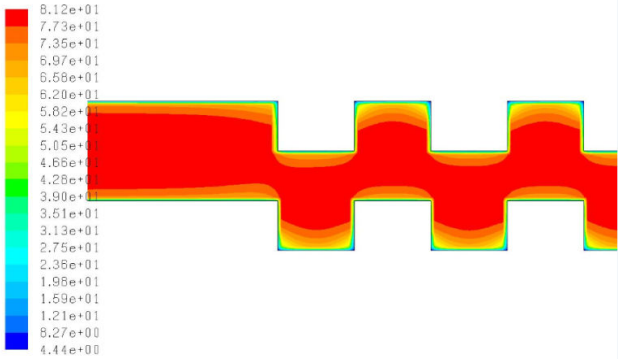

Fig. 49 Turbulence intensity at the middle of channel at Re 1400

Fig. 50 and 51 show the static temperature along the square corrugated channel for a constant wall temperature boundary condition at Reynolds numbers 400, and 1400.

As compared with triangular and sinusoidal corrugation channel, the temperature at the second valley has markedly decreased from 319K for both triangular and sinusoidal corrugation channel to 311K for square corrugated channel. Also, it is worth noting that the significant change happens at the corrugation area as shown in Fig. 52.

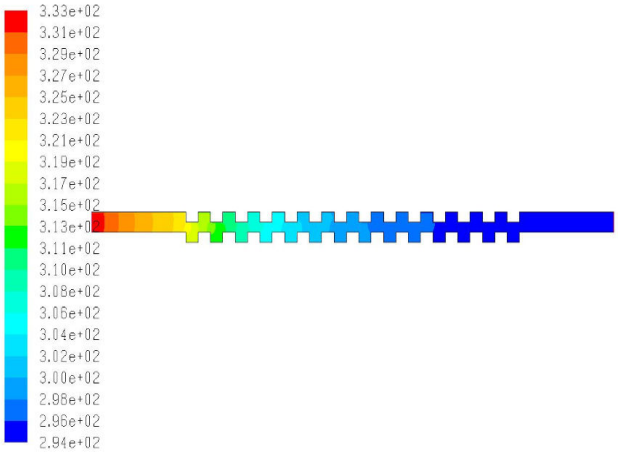

Fig. 50 Static temperature at Re 400

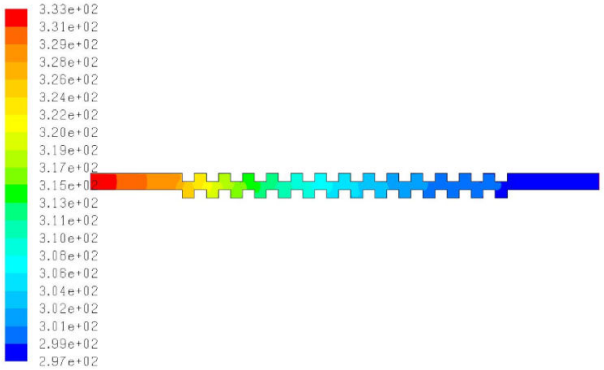

Fig. 51 Static temperature at Re 1400

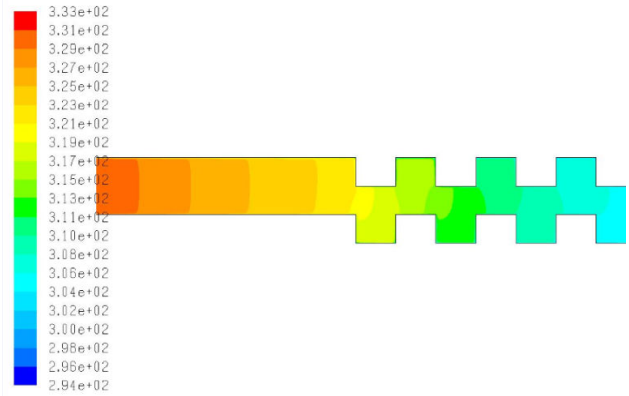

Fig. 52 Static temperature at the entrance part of the channel at Re 1400

E. Global Comparison Between the Triangular, Sinusoidal, and Square Corrugated Channels l

All the global values of pressure drop, wall shear stress, friction factor, heat flux, Nusselt number, and heat transfer coefficient were obtained by using the trapezoidal rule, as explained by [37], for the tabular local data resulted out of Fluent.

Fig. 53 compares the pressure drop for the triangular, sinusoidal, and square corrugated channels for the Reynolds number varying from 400 to 1400.

The important aspect of the graph is that the pressure drop for square corrugated channel rises gradually for the Reynolds number up to 1200 before it booms dramatically to reach a peak of 1500 Pascal.

Another aspect is that the pressure drop for both triangular and sinusoidal has slightly risen with just few Pascals.

The interesting observation is that while the pressure drop for triangular corrugation compared to sinusoidal corrugation, has increased with 17.5%, 38%, and 41.6% for Re 400, 1250, and 1400 respectively, the pressure drop for square corrugation is equal to 134, 151, and 188.6 folds of the pressure drop for the triangular corrugation within the same Reynolds numbers.

It can be justified that the pressure drop is firmly related to the configuration and severity of corrugation which promotes wall shear stress. As the corrugation changes smoothly, however, the pressure drop increases, but with inconsiderable values as extracted in the case of sinusoidal channel. When the severity of corrugation is getting sharp and sudden as of triangular and square channel, the pressure drop goes up with significant pace.

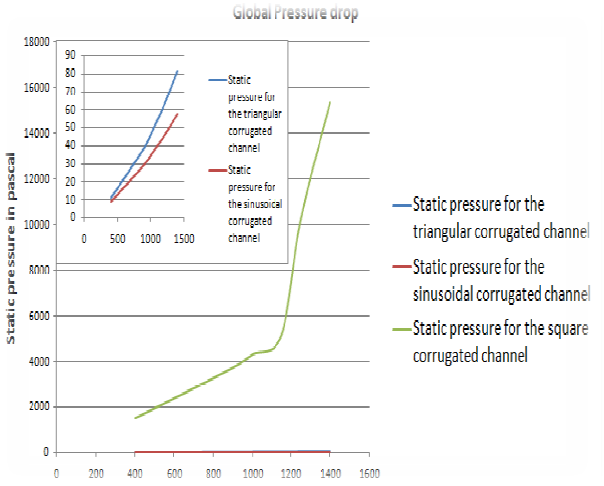

Fig. 53 Global pressure drop

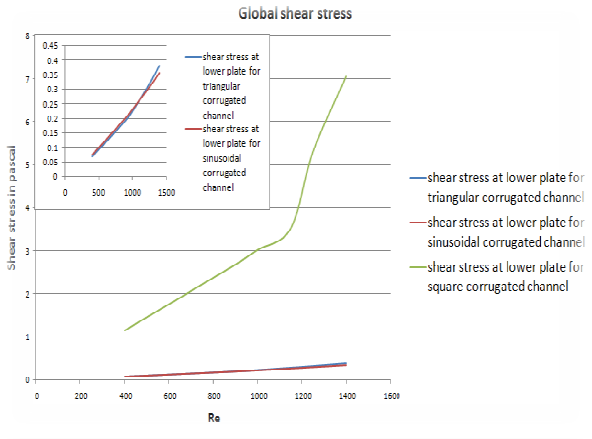

Fig. 54 Global shear stress

From the above graph, the values of shear stress for the square corrugation has increased with 16.2%, 16.6%, and 18.5% for Re 400, 1250, and 1400 respectively compared to the triangular corrugation.

This dissimilarity in shear stress can be ascribed to the variation of the change in momentum flow rate as the velocity profile develops.

Fig. 55 describes the relation between the friction factor for the lower plate of the triangular, sinusoidal, and square corrugated channel for the Reynolds number varying from 400 to 1400.

It is obvious that when the Reynolds number increases, the friction factor decreases, also, it can be seen that both the friction factor for triangular, and sinusoidal corrugation channel maintain almost the same slop in decreasing within a range of friction factor varies from 0.39 to 0.147, whereas the friction factor for square corrugated channel declines but more steeply within friction factor values begins at 5.848 and ends at 1.7.

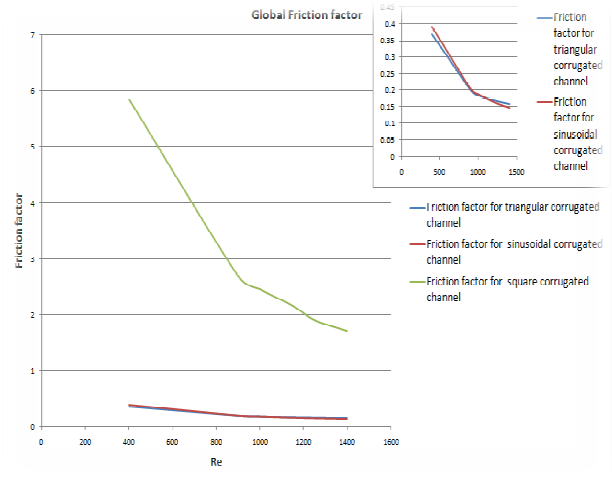

Fig. 55 Global friction stress

Fig. 56, 57, and 58 compare the heat flux, Nusselt number, and heat transfer coefficient respectively, for triangular, sinusoidal, and square corrugated channel for Reynolds number of 400, 900, 1150, 1250, and 1400.

The most salient point in the graphs is that as Reynolds number precedes the heat flux, Nusselt number, and heat transfer coefficient increase with similar behavior.

Fig.56, 58 show that both as heat flux and heat transfer coefficient for triangular corrugated channel increase 6.09% at Re 400, and 8.39% at Re 1400 compared to sinusoidal corrugated channel, the heat flux for square corrugated channel is equal to almost four times of the heat flux for triangular corrugated channel.

Similarly, the Nusselt number for triangular corrugated channel, as of Fig. 57, increases 3.97% at Re 400, and 6.21% at Re 1400 referred to sinusoidal corrugated channel, while the Nusselt number for square corrugated channel is equal to almost four times of that for triangular corrugated channel.

The increase of heat flux, Nusselt number and heat transfer coefficient as the configuration of corrugation varies, can be justified as it is stated hereinafter:

As the periodic changes in flow direction resulted in square surface corrugation is high, the created significant shear wall stress produces high pressure variability which, in turn, affects the velocity profile that is responsible of separating and reattachment of the flow boundary layer. This process leads to create large vortices producing turbulence flow that accelerates the velocity perpendicular to the wall. This velocity helps increase advection of fluid from the centre towards the side walls which in sequence enhances the heat transfer process for this region

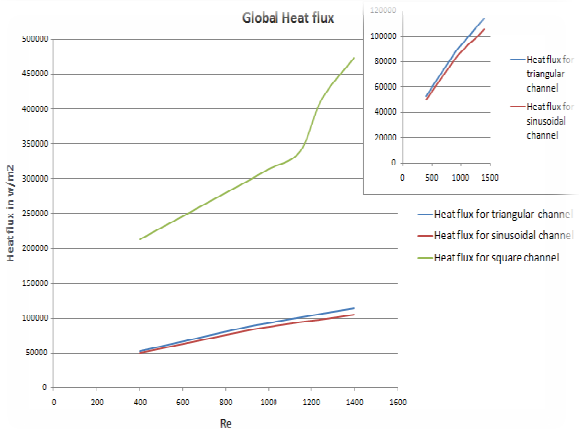

Fig. 56 Global heat flux

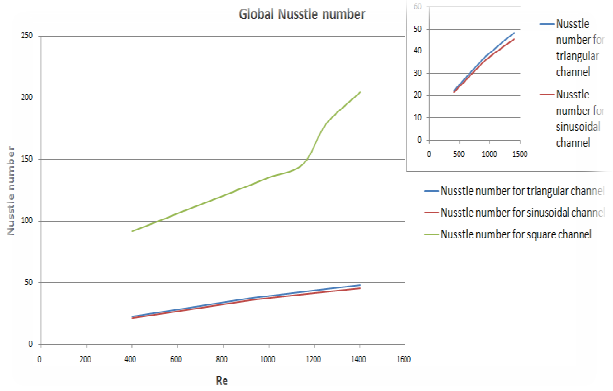

Fig. 57 Global Nusselt number

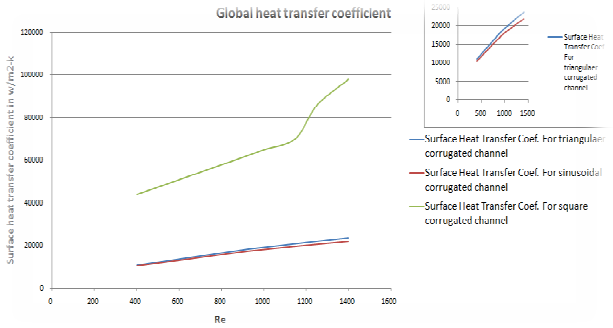

Fig. 58 Global heat transfer coefficient

F. Comparison Between Nusselt Numbers for Constant Wall Temperature and Constant Wall Heat Flux Boundary Conditions for the Triangular, Sinusoidal, and Square Corrugated Channels

In order to address the difference between the two boundary conditions, the assumption is made that the lower and upper plates consisting the corrugated channel are electrically cooled under the same heat flux. The electric cooling, as mentioned by [38], is the way which can realize the constant wall heat flux. This was done with the data obtained for the simulated corrugated channels under the constant wall temperature condition. The wall heat flux values computed for each corrugated channels under the constant wall temperature, were applied as a boundary condition for the case of constant wall heat flux. In order for the results to be with high accuracy, the heat flux values were computed directly from Fluent, instead of being extracted through the trapezoidal integration rule from the local data. The values of 13593.02, 13846.93, and 43589.336 W/m² were applied as constant heat flux boundary conditions for triangular, sinusoidal, and square corrugation channel respectively.

Fig.59, 60, and 61 show a comparison between Nusselt numbers for the constant wall temperature and constant wall hear flux for triangular, sinusoidal, and square corrugated channel with variation of Reynolds number from 400 to 1400.

The most noticeable feature is that the Nusselt number for constant wall heat flux is higher than of constant wall temperature. It can be seen that the Nusselt number for the triangular corrugated channel has increased 21.07% at Re 400, and then the difference has slightly diminished to reach 13.24% at Re 1400. Similar behavior has been observed for sinusoidal corrugated channel in which the Nusselt number has augmented with 21.6% at Re 400, and then declined to 15.6% at Re 1400.

For the square corrugated channel, the increment is substantial. The Nusselt number has doubled at the Re 400, and reached almost four times at Re 1400.

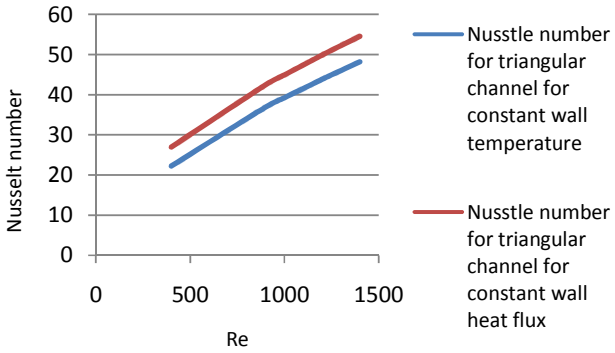

Fig. 59 Nusselt Number for triangular corrugated channel for two different boundary conditions

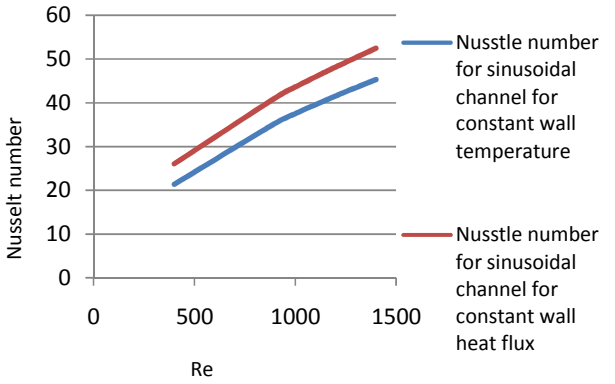

Fig. 60 Nusselt Number for sinusoidal corrugated channel for two different boundary conditions

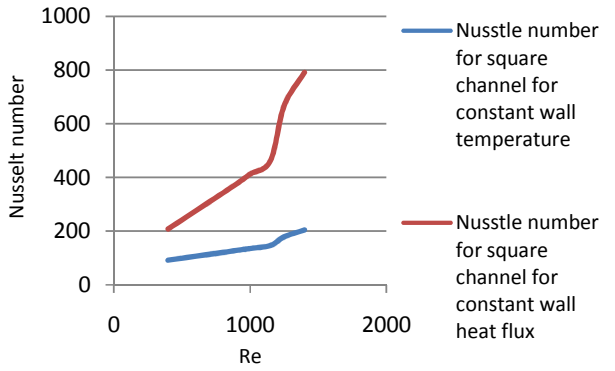

Fig. 61 Nusselt Number for square corrugated channel for two different boundary conditions

An increase in heat transfer rate can be contributed to the difference in thicknesses of the thermal boundary layers for each case. Fig. 62 compares between the thermal boundary layer thicknesses at constant wall temperature and constant wall heat flux boundary conditions for triangular corrugated channel at the entrance lower flat plate for Re 400.

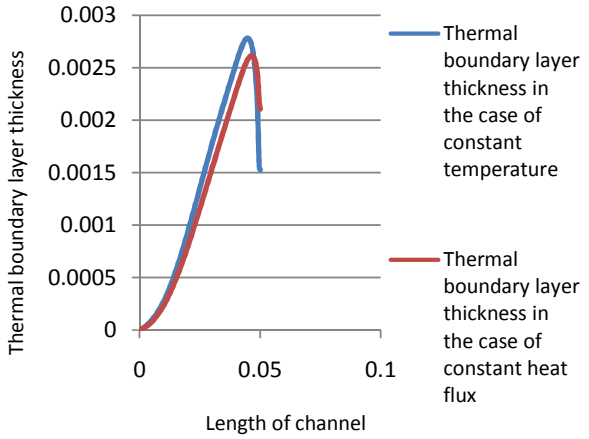

Fig. 62 Thermal boundary thickness for constant temperature and constant heat flux

IV. Conclusion

The main conclusions are stated hereinafter:

-The model mesh is very sensitive to the size and type of grid applied. Nusselt numbers for triangular corrugated channel at Re 400 with constant temperature boundary conditions for coarse mesh, fine regular mesh, and fine boundary layer mesh, were compared to the Nusselt number resulted from [2]. The study shows that the difference between results decreasing from +310.5% for coarse mesh to +160% for fine regular mesh, and then to +7.4% for fine boundary layer mesh. The latter was considered accurate enough for further simulations.

-The number of iteration is dependent upon the Reynolds number. As Reynolds number increases, the number of iteration decreases.

-As the water flows through the corrugated channel, the flow vortices are created. The vortex grows larger and its centre moves to the downstream as Reynolds number increases. The vortices generation is attributed to the pressure gradient within the periodic corrugations, which causes the flow velocity reduction. This trade off triggers flow separation and adverse motion, which produce vortices. The largest vortices are shown for square model, while the smallest are visualized for sinusoidal model.

-The pressure drop is reliant to the Reynolds number and to the pattern of corrugated surface. With increasing of Reynolds number, the pressure drop increases as well. As the Reynolds number is a function of the flow velocity, it is observed for triangular corrugated channel that if the inlet velocity increases 125% the pressure drop increases 233.3%. Globally, for Re 400, the pressure drop increases 17.5% in the triangular model compared to sinusoidal model, while the pressure drop for square model is equal to 134 times of triangular model.

-The turbulence intensity is also affected by both Reynolds number and corrugation pattern. When the inlet velocity for triangular corrugated channel raises to 250% at a specified location i.e. the second valley of the channel, the turbulence intensity ascends from 8.3% to 16.3%. The highest turbulence intensity is observed for square model, and the lowest intensity is shown for sinusoidal model.

-The shear stress increases as a consequence of Reynolds number increasing. The highest value of shear stress obtained at the peak of corrugation. From global point of view for Re 400, the shear stress for the square model has increased with 16.2 compared to the triangular model.

-The friction factor is adversely related to Reynolds number. When the Reynolds number goes up, the friction factor declines. Also, is noticeable that the highest value of friction factor occurs at the peak of corrugation. For Re 400, the friction factor increases from just 0.39 for triangular and sinusoidal models to 5.84 for square model.

-With progression with Reynolds number, the heat transfer rate sensibly increases. This can be measured by increasing of Nusselt number for triangular corrugated channel from 36.9 at Re 900 to 48.17 at Re 1400. Compared to sinusoidal and square models at Re 400, the Nusselt number for triangular model increases 3.97% referred to sinusoidal model, while Nusselt number for square model is equal to about four times of that for triangular model.

-The cooling by electric method .i.e. constant wall heat flux is more efficient than the cooling by fluid method .i.e. constant wall temperature. For Re 400, the Nusselt number increases 21.07%, 21.6%, and four times for triangular, sinusoidal, and square respectively.

From above all, it is concluded that both hydrodynamic and thermal behaviors are strictly relevant to Reynolds number and the pattern of corrugation. To sum up, in order to increase Nusselt number only one time (thermal energy) by altering the surface plate patterns, the pressure drop increases 33.5 times (mechanical energy), and as the mechanical energy is worth four to ten times as much as its equivalent in heat in thermal power system as it was mentioned in [22], the designer should seek the compromised solution which realizes low spending for mechanical energy while keeping the thermal energy high.

Acknowledgment

The author would like to thank Sirte Oil Company and his family for supporting all the time and helping to maintain enthusiasm in completing this paper.

References

[1] Kanaris, A., G., Mouza, A., A., and Paras, S., V. (2009)' Optimal design of a plate heat exchanger with undulated surfaces', *Chemical Engineering Research and Design*, 83(5), pp. 1184-1195. Science Direct [Online]. Available at: www.siencedirect.com.

[2] Kanaris, A., G., Mouza, A., A., and Paras, S., V. (2005)' Flow and Heat Transfer in Narrow Channels with Corrugated Walls: A CFD Code

Application', *Chemical Engineering Research and Design*, 83(5), pp. 460-468. Science Direct [Online]. Available at: www.siencedirect.com.

[3] Kanaris, A., G., Athanasios, G., Mouza, A., A., Aikaterini, A., Paras, S., V., Spiros V. (2006)' Flow and heat transfer prediction in a corrugated plate heat exchanger using a CFD code', *Chemical Engineering and Technology*, 29(8), pp. 923-930. Compedex [Online]. Available at: www.interscience.wiley.com.

[4] Yasar, I., and Cem, P. (2003)' The effect of channel height on the enhanced heat transfer characteristics in a corrugated heat exchanger channel', *Applied Thermal Engineering*, 23(8), pp. 979-987. Science Direct [Online]. Available at: www.siencedirect.com.

[5] Choi, J. M. and. Anand, N. K. (1995)' Turbulent heat transfer in a serpentine channel with a series of right-angle turns', *International Journal of Heat and Mass Transfer*, 38(7), pp. 1225-1236. Science Direct [Online]. Available at: www.siencedirect.com.

[6] Wang, G., and Vanka, S. P. (1995)' Convective heat transfer in periodic wavy passages', *International Journal of Heat and Mass Transfer*, 38(17), pp. 3219-3230. Science Direct [Online]. Available at: www.siencedirect.com.

[7] Sawyersa, D. R., Sen, M., Hsueh, and Chang (1998)' Heat transfer enhancement in three-dimensional corrugated channel flow', *International Journal of Heat and Mass Transfer*, 41(22), pp. 3559-3573. Science Direct [Online]. Available at: www.siencedirect.com.

[8] Nishimura, T., Matsune, S. (1998)' Vortices and wall shear stresses in asymmetric and symmetric channels with sinusoidal wavy walls for pulsatile flow at low Reynolds numbers', *International Journal of Heat and Fluid Flow*, 19(6), pp. 583-593. Science Direct [Online]. Available at: www.siencedirect.com.

[9] Gao, WF; Lin, WX; Lu, and ER. (2000)' Numerical study on natural convection inside the channel between the flat-plate cover and sine-wave absorber of a cross-corrugated solar air heater', *Energy Conservation Management*, 41(2), pp. 145-151. Science Direct [Online]. Available at: www.siencedirect.com.

[10] Mehrabian, M. A., Poulter, R. (2000)' Hydrodynamics and thermal characteristics of corrugated channels: Computational approach', *Applied Mathematical Modelling*, 24(5-6), pp. 343-364. Compendex [Online]. Available at: www.siencedirect.com.

[11] Nieno, B., and Nobile, E. (2001)' Numerical analysis of fluid flow and heat transfer in periodic wavy channels', *International Journal of Heat and Fluid Flow*, 22(2), pp. 156-167. Science Direct [Online]. Available at: www.siencedirect.com.

[12] Zimmerer, C., Gschwind, P., Gaiser, G., and Kottke, V. (2002)' Comparison of heat and mass transfer in different heat exchanger geometries with corrugated walls', *Experimental Thermal and Fluid Science*, 26(2-4), pp. 269-273. Science Direct [Online]. Available at: www.siencedirect.com.

[13] Hossain, M. Z., Islam, A.K.M., and Sadrul (2004)' fully developed flow structures and heat transfer in sine-shaped wavy channels', *International Communications in Heat and Mass Transfer*, 31(6), pp. 887-896. Compendex [Online]. Available at: www.siencedirect.com.

[14] Zhang, J., Kundu, J., and Manglik, R. M. (2004)' Effect of fin waviness and spacing on the lateral vortex structure and laminar heat transfer in wavy-plate-fin cores', *International Journal of Heat and Mass Transfer*, 47(8-9), pp. 1719-1730. Science Direct [Online]. Available at: www.siencedirect.com.

[15] Metwally, H. M. and Manglik, R. M. (2004)' Enhanced heat transfer due to curvature-induced lateral vortices in laminar flows in sinusoidal corrugated-plate channels', *International Journal of Heat and Mass* Transfer, 47(10-11), pp. 2283-2292. Science Direct [Online]. Available at: www.siencedirect.com.

[16] Manglik, R. M., Zhang, J., and Muley, A. (2005)' Low Reynolds number forced convection in three-dimensional wavy-plate-fin compact channels: Fin density effects', *International Journal of Heat and Mass Transfer*, 48(8), pp. 1439-1449. Science Direct [Online]. Available at: www.siencedirect.com.

[17] Nathan, R., Rosaguti, David, F., Fletcher and Brian, S. H, (2007)' Low-Reynolds number heat transfer enhancement in sinusoidal channels', *Chemical Engineering Science*, 62(3), pp. 694-702. Science Direct [Online]. Available at: www.siencedirect.com.

[18] Tao, Y. B., He, Y. L., Huang, J., Wu, Z. G., and Tao, W. Q. (2007)' Three-dimensional numerical study of wavy fin-and-tube heat exchangers and field synergy principle analysis', *International Journal of Heat and Mass Transfer*, 50(5-6), pp. 1163-1175. Science Direct [Online]. Available at: www.siencedirect.com.

[19] Ko, T. H. (2007)' A numerical study on developing laminar forced convection and entropy generation in half- and double-sine ducts', *International Journal of Thermal Sciences*, 46(12), pp. 1275-1284. Compendex [Online]. Available at: www.siencedirect.com.

[20] Pham, M. V., Plourde, F., and Doan, S. K. (2008)' Turbulent heat and mass transfer in sinusoidal wavy channels', *International Journal of Heat and Fluid Flow*, 29(5), pp. 1240-1257. Science Direct [Online]. Available at: www.siencedirect.com.

[21] Ismail, S. L., Ranganayakulu, C., and Ramesh K. S. (2009)' Numerical study of flow patterns of compact plate-fin heat exchangers and generation of design data for offset and wavy fins', *International Journal of Heat and Mass Transfer*, 52(17-18), pp. 3972-3983. Science Direct [Online]. Available at: www.siencedirect.com.

[22] Kays, W, and London, A., L. (1964) *compact heat exchangers*. 2nd edn. New Youk: McGraw-Hill.

[23] Heggs, J., Sandham, P., Hallam, R. A., and Walton, C. (1997)' Local Transfer Coefficients in Corrugated Plate Heat Exchanger Channels', *Chemical Engineering Research and Design*, 75(7), pp. 641-645. Science Direct [Online]. Available at: www.siencedirect.com.

[24] Drosos, E. I. P., Mouza, A. A., Paras, s. V., and Karabelas, A. J. (2002) *E.K.E.T.A.*. Available at: http://library.certh.gr/libfiles/PDF/AIK-CPERI-1ST-WRKSP-Y2002-PP39-42.pdf.

[25] Vlasogiannis, P., Karagiannis, G., Argyropoulos, P., and Bontozoglou, V. (2002) *citeULike*. Available at: http://www.citeulike.org/user/Francke/article/4631512.

[26] Lioumbas, I.S., Mouza, A.A.; Paras, S.V (2002)' Local velocities inside the gas phase during counter-current two-phase flow in a narrow vertical channel', *Chemical Engineering Research and Design*, 80(6), pp. 667-673. Compendex [Online]. Available at: www.siencedirect.com.

[27] Versteeg, H, K. (1995) *an introduction to computational fluid dynamics: the finite volume method*. Harlow: Longman.

[28] Naphon, P., and Kornkumjayrit, k. (2008)' Numerical analysis on the fluid flow and heat transfer in the channel with V-shaped wavy lower plate', *International Communications in Heat and Mass Transfer*, 35(7), pp. 839-843. Science Direct [Online]. Available at: www.siencedirect.com.

[29] Fernndez, J. A., Elicer-Corts, J. C., Valencia, A., Pavageau, M., and Gupta, S. (2007)' Comparison of low-cost two-equation turbulence models for prediction flow dynamics in twin-jets devices', *International Communications in Heat and Mass Transfer*, 34(5), pp. 570-578. Science Direct [Online]. Available at: www.siencedirect.com.

[30] Shah, R. K. (1978) *Laminar flow for forced convection in ducts: a source book compact heat exchanger analytical data*. London: Academic press.

[31] Holman, J. P. (1992) *Heat Transfer*. 7th edn. London: McGraw-Hill.

[32] Aishuang, X., and Songlin, X. U. (2005) *SpringerLink*. Available at: http://www.springerlink.com/home/main.mpx.

[33] Guo1, H. F., Chen, Z. Y., Yu, C. W. (2008) *Institute of Physics*. Available at: http://www.iop.org/.

[34] Zhipeng, L., and Zhengming, G., (2008) *International Symposium on Mixing in Industrial Processes VI*. Available at: http://www.ismip6.polymtl.ca/docs/5-11.pdf.

[35] Mangesh, K., and Yavuzkurt, S. (2009) *International centre for heat and mass transfer*. Available at: http://www.ichmt.org/turbine-09/images/abstracts/11.pdf.

[36] Martin, H. (1996)' A theoretical approach to predict the performance of chevron-type plate heat exchangers', *Chemical Engineering and Processing*, 35(4), 301-310. Science Direct [Online]. Available at: www.siencedirect.com.

[37] Liengme, B. V. (2002) *guide to Microsoft Excel 2002 for scientists and engineers*. 3rd end. Oxford: Butterworth-Heinemann

[38] Darabi, J., Ohadi, M. M., Fanni, M. A., Dessiatoun, S. V., Kedzierski, M. A. (1999) Fire on the Web. Available at: http://www.fire.nist.gov/bfrlpubs/build99/PDF/b99054.pdf.